Unravelling surface changes on Cu-Ni alloy upon immersion in aqueous media simulating catalytic activity of aerobic biofilms

Nesrine Aissaoui, Irma Liascukiene, Michel Genet, Christine Dupont-Gillain, Karim El Kirat, Caroline Richard, Jessem Landoulsi

Version of Record: https://www.sciencedirect.com/science/article/pii/S0169433219328971
Manuscript_f3a912d01494d02e0704a729bcbff664

Unravelling surface changes on Cu-Ni alloy upon immersion in aqueous media simulating catalytic activity of aerobic biofilms

Nesrine Aissaoui [a,†‡], Irma Liascukiene [b,†], Michel J. Genet [c], Christine Dupont-Gillain [c], Karim El Kirat [d], Caroline Richard [e], Jessem Landoulsi [b *]

[a] *Department of Chemistry and Chemical Engineering, Chalmers University of Technology, Gothenburg, Sweden*

[b] *Sorbonne University, CNRS, UMR 7197, Laboratory of Surface Reactivity (LRS), F-75005, Paris, France.*

[c] *Institute of Condensed Matter and Nanosciences, Bio & Soft Matter, Université catholique de Louvain, Place Louis Pasteur 1 Box L4.01.10, B-1348 Louvain-la-Neuve, Belgium*

[d] University of Technology of Compiègne, Biomechanics & Bioengineering, CNRS, UMR 7338, Rue Personne de Roberval, 60200 Compiègne, France

[e] *University of Tours, GREMAN, CNRS, UMR 7347, 37200, Tours, France*

* Corresponding author: jessem.landoulsi@sorbonne-universite.fr

Tel. +33 1 44 27 54 52

† These authors contributed equally.

‡ Present address: Center of Structural Biochemistry, INSERM U1054, CNRS UMR 5048, University of Montpellier, 34090, Montpellier, France.

Abstract

Cu-Ni alloys are extensively used in contact with natural waters and are impacted by microbial activities of biofilms. The mechanisms by which surface changes occur upon immersion remain not well understood. Herein, an aerobic microbial activity of natural biofilms is mimicked by the enzymatic generation of an oxidizing agent and an organic acid. Surface changes are probed through a detailed analysis of XPS spectra which allowed a distinction between compounds of organic and inorganic nature to be made. Results show that the surface is composed of copper oxides/hydroxides, presumably Cu_2O and $Cu(OH)_2$ and Ni hydroxides. The enzyme-catalyzed reaction causes a significant depletion of Ni and inorganic oxygen, while the concentration of copper, Cu^{I} and Cu^{II}, vary only slightly. Surface changes concern the organic phase; the amount of organic compounds strikingly increases in the presence of enzymes, and the XPS spectra reveal the accumulation of compounds with high oxidized carbon content, attributed to adsorbed gluconate. Correlations between spectral data suggest the formation of Cu-gluconate complex, probably through coordinative bonds between gluconates and Cu^{II} on the oxide layer. These findings are particularly important to properly evaluate the impact of microbial activities on the sustainability of Cu-Ni alloys upon natural exposures.

1. Introduction

In wet non-sterile media, the performances of metallic materials may be strongly impacted by the presence of microorganisms on their surfaces, causing significant economic consequences, particularly for structures located in natural waters, such as cooling circuits, ships and related equipment. Microorganisms may indeed adhere on material surfaces and grow to form biofilms which change the physicochemical conditions at the metal/solution interface in different ways, depending on the microorganisms' species, the properties of material surfaces, the conditions of exposure, etc. [1-4] Microorganisms can either induce or accelerate corrosion, while in some cases, they may, surprisingly, reduce this process. [1-4] This effect seems to be achieved by the action of extracellular polymeric substances (EPS). It has moreover been shown that the biogenic formation of an oxidizing agent may inhibit pits' propagation on stainless steel surface. [5]

Copper-nickel alloys (Cu-Ni), also called cupronickels, are frequently utilized in many structures in contact with marine and freshwater environments such as heat exchangers required in power plants, cladding material for ship hulls and offshore structures. This is due to the remarkable thermal conductivity of these materials and their good resistance to corrosion. [6] For instance, the high copper content of the Cu-Ni alloy makes it more relevant than galvanized or epoxy-coated mild steel for utilization in piping systems. When exposed to such humid and non-sterile media, Cu-Ni alloys may be colonized by a variety of microorganisms, which adhere and grow to form biofilms and may lead to the degradation of the material. [7] The microbiologically-influenced corrosion (MIC) of Cu-Ni alloys has been the subject of numerous studies but remains less documented compared to the one of stainless steels. [6, 8, 9] Some papers have reported MIC processes of Cu-Ni alloys in the presence of aerobic bacteria in seawater, showing an acceleration of the corrosion rates. [10-12] In aerobic conditions, it has been shown that the biogenic production of hydrogen peroxide (H_2O_2) plays

a pivotal role in MIC processes (see [8] and references therein). This is due to the metabolic activities of heterotroph aerobic bacteria which use oxygen as electron acceptor to form highly reactive species (reactive oxygen species, ROS) such as H_2O_2, at the crossroad of many enzymatic reactions. [8] The biofilms formed in natural waters can generate H_2O_2 with a concentration lower than ~3 mmol/L. [13-15] Therefore, there has been a growing interest to use purified enzymes in MIC studies with the aim to mimicking aerobic activities within natural biofilms. [8]

Glucose oxidase (GOx, EC 1.1.3.4) is an enzyme that belongs to the class of oxidoreductases and catalyzes the formation of H_2O_2 by conversion of D-glucose into gluconolactone (Eq. 1) which is spontaneously converted into gluconic acid.

$$\text{D-Glucose } (C_6H_{12}O_6) + O_2 + H_2O \rightarrow \text{D-Glucono-1,5-lactone } (C_6H_{10}O_6) + H_2O_2 \quad (1)$$

The relevancy of this biomimetic system has been proven in MIC studies dealing with the behavior of stainless steels in natural waters. [16] Indeed, glucose, the substrate of GOx, is present in natural waters, and has been detected in a significant amount in biofilms formed upon natural exposure of metallic materials. [17] Furthermore, the generation of H_2O_2 may be modulated while taking into account the physicochemical conditions simulating natural exposures (natural diffusion, pH, ionic strength, etc) by adjusting the amounts of the enzyme and its substrate, yielding concentrations of few mmol/L. [18] In a previous study, it has been shown that the abrupt addition of H_2O_2 in the media or its *in situ* generation by enzymes induces changes on stainless steel surface which are radically different. [18] This suggests that kinetics of MIC processes must be considered in the design of laboratory-controlled tests used to evaluate the resistance of materials.

The aim of the present work is to probe surface changes of a Cu-Ni (90/10) alloy, also designated as 90Cu-10Ni, upon immersion in aqueous medium simulating aerobic microbial activity. 90Cu-10Ni is an alloy containing approximately 90% copper and 10% nickel and

small additions of iron and manganese. This alloy is one of the main materials used for piping systems as it exhibits a sufficient mechanical strength and good ductility. Importantly, it may not require cathodic protection owing to its good resistance to corrosion and erosion-corrosion. However, the evolution of the surface composition of this alloy in the presence of microbial activities remain poorly documented. In the present study, a particular attention is dedicated to the identification of inorganic compounds (oxide layer) and bio-organic species possibly adsorbed on the material surface. For this purpose, X-ray photoelectron spectroscopy (XPS) is used to decipher changes induced by the enzyme-catalyzed reaction or one of its products, i.e. H_2O_2 and gluconic acid, on the surface composition.

2. Materials and methods

2.1. Materials and solutions

Squares of 90Cu-10Ni (1 cm × 1 cm, thickness ~1mm, from KM Europe Metal AG) were used for this study. The chemical bulk composition of the alloy is given in Table 1. The samples were mechanically polished with SiC papers of 600 and 1200 grain size (both sides and perimeter) followed by fine polishing with successive 6, 3, and 1 µm diamond suspensions (Struers, France). The samples were rinsed in binary mixtures of ultrapure water/ethanol (50%/50%) in a sonicating bath (70 W, 40 kHz, Branson, USA), then dried under nitrogen gas flow. All experiments were performed in "synthetic fresh water" (SFW, NaCl 0.46 mmol/L, Na_2SO_4 0.26 mmol/L, $NaNO_3$ 0.2 mmol/L, $NaHCO_3$ 3.15 mmol/L, pH ~8) at room temperature. All the above chemicals were provided by Sigma-Aldrich (France) ensuring 99% minimum purity. Ultrapure water was produced by Millipore technology (MilliQ, Millipore, France).

Glucose oxidase (Gox, EC 1.1.3.4, 47200 U/g)1 from *Aspergillus Niger*, Peroxidase (EC 1.11.1.6, 2860 U/g solid) from bovine liver, D-glucose and hydrogen peroxide (30 % wt.) were purchased from Sigma-Aldrich and used without further purification. After surface

preparation, 90Cu-10Ni samples were introduced in a 100mL open reactor and positioned horizontally in the bottom. The samples were incubated for five days in one of the following medium (Table 2), at room temperature (~22-24°C):

"SFW": synthetic fresh water,

"H_2O_2": SFW containing 2 mmol/L hydrogen peroxide,

"GAc": SFW containing 2 mmol/L gluconic acid,

"GOx: SFW containing *D*-glucose (20 mmol/L) and glucose oxidase (200 U/L).

After incubation, the samples were thoroughly rinsed with ultrapure water and dried under nitrogen gas flow.

2.2. Enzyme activity

The evolution of GOx activity was examined by monitoring H_2O_2 production with a colorimetric assay. A peroxidase was used to catalyze the consumption of H_2O_2 by oxidizing the 2,2-azino-bis(3-ethylbenzothiazoline-6-sulfonic) acid (ABTS) into $ABTS^{\bullet+}$ radical cation as follows:

$$H_2O_2 + ABTS \rightarrow 2H_2O + ABTS^{\bullet+} \qquad (2)$$

For this purpose, a sample (100 µL) is taken from the incubation medium (for H_2O_2 or GOx media) at a given time and immediately placed in an ice bath to stop the glucose oxidase activity (only for GOx medium). The sample was then introduced in a cuvette (3mL) containing ABTS solution (acetate buffer, 50 mM, pH = 5.1). Peroxidase is finally added in the cuvette its activity was evaluated by monitoring $ABTS^{\bullet+}$ production (reaction 2) at room temperature (~22-24°C). The $ABTS^{\bullet+}$ concentration was determined by measuring the absorbance at 414 nm using a UV spectrophotometer (6715 Jenway, UK). A calibration curve was preliminarily established to relate the activity of peroxidase (initial velocity) to H_2O_2 concentration.

The enzymatic activity was also evaluated by monitoring the pH variation, due to the production of gluconic acid, and the concentration of dissolved O_2 (see reaction 1). Dissolved oxygen concentration in the solutions was examined using an oxygen probe (BPL Inolab, WTW, Germany) equipped with an integrated stirrer.

2.3. XPS analysis

XPS analyses were performed using a Kratos Axis Ultra spectrometer (Kratos Analytical, UK), equipped with a monochromatized aluminum X-ray source (hν = 1486.74 eV) (powered at 10 mA and 15 kV) and an eight channeltrons detector. Charge stabilization was insured by using an electron source (filament current set at 1.9 A, bias 1.2 eV) mounted coaxial to the lens column and a charge balance plate (voltage set at 3.5 V). Analyses were performed in the hybrid lens mode with the slot aperture, the analyzed area being about 0.7 mm x 0.3 mm. The pass energy was set at 160 eV for the survey spectrum and 40 eV for narrow scans. In the latter conditions, the full width at half maximum (FWHM) of the Ag $3d_{5/2}$ peak of a standard silver sample was about 0.9 eV. The angle between the normal to the sample surface and the direction of photoelectron collection was 0. The pressure in the analysis chamber was around 10^{-6} Pa. The following sequence of spectra was recorded: survey spectrum, C 1s (start), O 1s, N 1s, Cu 2p, Ni 2p, C 1s (intermediate), Fe 2p, Cl 2p, $L_3M_{45}M_{45}$ and C 1s (final). The C 1s peak was recorded in the beginning, in the middle and at the end of the sequence to check the stability of sample charging and the absence of organic compounds degradation as a function of time. This procedure showed the need of using a flood gun to stabilize the surface charge because the surface of these thick specimens is probably not as conductive as the bulk. The binding energy scale was set by fixing the C 1s component due to carbon only bound to carbon and hydrogen at 284.8 eV. The data treatment was performed with the Casa XPS software (Casa Software Ltd., UK). Unless stated otherwise, the peaks were decomposed using a linear baseline, and a component shape defined by the product of a Gauss and Lorentz

function, in the 70:30 ratio, respectively. Molar concentration ratios were calculated using peak areas normalized according to the acquisition parameters and the relative sensitivity factors and transmission function provided by the manufacturer. Three independent sets of samples were analyzed to evaluate the reproducibility.

2.4. Polarization-modulation infrared reflection absorption spectroscopy (PM-IRRAS)

PM-IRRAS is a non-destructive physicochemical analysis, which is convenient for the characterization of thin films deposited on metal substrates. This method utilizes light whose polarization is modulated; it is continually alternated between p- and s- polarizations by means of a photo-elastic modulator (PEM). In the condition of near specular reflection, s-polarization and the main component of p-polarization are parallel and perpendicular to the sample surface, respectively [19]. The p-polarization includes information about the adsorbed compounds on the surface and in the gas phase, whereas the s-polarization includes information about only the gas phase. The PM-IRRAS spectrum is thus obtained by dividing the measured difference reflectivity ($R_p - R_s$) by the sum reflectivity ($R_p + R_s$), where R_p and R_s are the intensity of the p-polarized and s-polarized component of the radiation, respectively. In this work, PM-IRRAS spectra were recorded on a commercial Nexus spectrometer (Thermo-Scientific, France). The external beam was focused on the sample with a mirror, at an optimal incident angle of 80°. A ZnSe grid polarizer and a ZnSe PEM, modulating the incident beam between p- and s-polarizations (HINDS Instruments, PEM 90, modulation frequency = 37 kHz), were placed prior to the sample. The light reflected at the sample was then focused onto a nitrogen-cooled MCT detector. All the spectra presented were obtained from the sum of 128 scans and the band positions are estimated to have a 8 cm^{-1} resolution.

3. Results and discussion

3.1. Composition and physicochemical properties of the media

The impact of the enzymatic activity in the aqueous solution was measured by monitoring the evolution of three key parameters: pH, concentration of H_2O_2, and dissolved O_2 over time as presented in Fig. 1. It is shown that the pH was stable in SFW at values ranging from 7.8 to 8.2 due to the presence of HCO_3^- ions in a significant amount (Fig. 1A). In presence of *D*-glucose and GOx, the pH decreased rapidly to reach a plateau at values ranging from 7.0 to 7.4. This pH drop is attributed to the production of gluconolactone, yielding gluconic acid, by the enzymatic reaction (Eq. 1). The evolution of the concentration of H_2O_2, generated by the GOx-catalyzed reaction, is presented in Fig. 1B, showing a progressive increase during the first day to reach about 2 mmol/L. Then, the rate of H_2O_2 production decreased over time reflecting a decrease in the kinetic of the enzymatic reaction, owing to the process of auto-inactivation [20, 21]. A concentration around 2 mmol/L is however maintained during a period of 5 days. In Fig. 1C, the concentration of dissolved O_2 concentration in SFW, without enzyme, was unchanged for 5 days, as expected. The mean measured values are in agreement with Henry's law describing the equilibrium at the air/water interface. However, in the GOx medium, most of the dissolved O_2 was consumed (typically > 99% of concentration decrease) during the first minutes of immersion, suggesting that the dissolved oxygen is consumed in the GOx-catalyzed reaction (Eq. 1). This indicates that in natural diffusion conditions, i.e. without stirring, the enzymatic reaction is kinetically limited by the dissolution of O_2 from the air. When the enzymatic activity decreased, due to the process of auto-inactivation, the concentration of dissolved oxygen increased progressively to reach a plateau, after four days, corresponding to the value measured in SFW without enzymes. Data describing the characteristics of the media used for incubation tests are summarized in Table 2.

3.2. XPS spectral data and chemical functions

Typical C 1s and O 1s peaks recorded on the different samples are presented in Fig. 2. The decomposition of these peaks was performed on the basis of the methodology developed for a

variety of inorganic materials used in applications with biological interest. [10, 22-24] C 1s peak can be confidently decomposed into four contributions: (i) a component at 284.8 eV due to carbon only bound to carbon and hydrogen [**C**–(C,H], (ii) a component at about 286.3 eV due to carbon bound to oxygen or nitrogen [**C**–(O,N)], including alcohol, amide, acetal or hemiacetal, (iii) a component at about 288 eV due to carbon making one double bond [**C**=O] or two single bonds with oxygen [O–**C**–O], including amide, acetal and hemiacetal, and finally (iv) a component near 289 eV due to carboxylic acid and ester (O=**C**–O). All components were constrained to have the same full width at half maximum (FWHM). The molar fractions associated with these components are given in Table 3.

The decomposition of the O 1s peak is less reliable than the one of the C 1s peak due to the presence of a series of very near components. Nevertheless the O 1s peak was tentatively decomposed in three components, on the basis of a previous procedure. [22] The first one at ~529.7 eV was attributed to inorganic oxygen in metal oxides, in agreement with the peak positions observed for Cu and Ni oxides. [25] The FWHM of the two other components were imposed to be equal. The component at about 531.2 eV may be due to [C=**O**] bonds (amide and carboxyl groups) or O atoms of carboxylate. The contribution due to the presence of metal hydroxides [M–**O**H] overlaps with this component. [26] The last component, at 533.1 eV, can be attributed to oxygen singly bound to carbon ([C–**O**–H] of alcohol and carboxyl, [C–**O**–C] of ether and ester).

The N 1s peak showed a main contribution at about 399.8 eV (not shown) which was attributed to amide or amine (**N**–C). No component at higher binding energy was clearly noticeable, indicating the absence of a significant amount of protonated amines.

The Cu $2p_{3/2}$ peak of the Cu 2p doublet shown in Fig. 3 was decomposed into two components attributed to Cu^0/Cu^I and Cu^{II}, respectively and two satellites. The distance between Cu $2p_{3/2}$ and Cu $2p_{1/2}$ peaks of the Cu 2p doublets was fixed at 19.85 eV [27], and a

ratio of 2 was imposed between their areas (not shown). The contribution at ~932.3 eV may be assigned to Cu^0 and/or Cu^I species. The contribution at about 934.4 eV was attributed to Cu^{II} species and was accompanied by two satellites at ~942 and ~944 eV, typical for Cu^{II} compounds, which were computed in the Cu^{II} mole fraction. [26, 28, 29] This contribution is more probably due to $Cu(OH)_2$ rather than CuO [30, 31] for which Cu $2p_{3/2}$ peak is reported close to 933.8 eV (see Table 4 for more details). [32]

The discrimination between Cu^0 and Cu^I species is not possible using the Cu $2p_{3/2}$ peak, as their binding energies are similar. This may be achieved using the modified Auger parameter, $\alpha' = E_K (C'C''C''') + E_B (C)$, proposed by Wagner [33] to probe changes in the local environment of the ionized atom, where E_K (C'C''C''') is the kinetic energy of an Auger transition involving C', C'', and C''' core electron levels and E_B (C) the binding energy of the corresponding XPS peak. Importantly, this parameter is insensitive to charging effects and changes in Fermi level. [34] Representative $CuL_3M_{45}M_{45}$ Auger peaks recorded on the 90Cu-10Ni samples after incubation in the different media are presented in Fig. 3. The values of α'_{Cu}, calculated by using the Cu $2p_{3/2}$ components (either at the lower or higher binding energy) and the Cu LMM Auger peak, are given in Table 4 and compared to data from the literature. Results clearly support the attribution of the component at ~932.3 to Cu^I compounds, presumably in Cu_2O, thus suggesting that Cu^0 was not detected by XPS. The molar fractions associated with these components are given in Table 3.

The Ni $2p_{3/2}$ peak of the Ni 2p doublet was used for quantification (Fig. 3), it exhibited a main contribution at ~855.8 eV with a satellite at ~ 861.7 eV which were both taken into account to calculate the Ni fraction. [29] This contribution was attributed to Ni^{II} in $Ni(OH)_2$ [31, 32, 35, 36] and probably not in NiO for which values reported in the literature are below 855.6 eV.[25] Values of 855.6 and 855.9 eV for NiOOH are also reported,[25] so the presence of NiOOH

cannot be totally excluded. A component at about ~852.2 eV, due to non-oxidized nickel (Ni^0), was not observed in this study.

Iron is also an alloying element in the 90Cu-10Ni alloy (Table 1). The surface concentration in iron cannot however be determined by XPS on this type of sample because the main Fe $2p_{3/2}$ peak at about 710 eV is overlapped with the Ni KL_1L_{23} (~709 eV), Ni $L_3M_{23}M_{45}$ (~715 eV) and Cu $L_2M_{23}M_{23}$ (~712 eV) Auger peaks. The two times less intense Fe $2p_{1/2}$ peak (~723 eV) is overlapped with Cu $L_3M_{23}M_{23}$ (~719 eV) and the five times less intense Fe 2s peak (~847 eV) is overlapped with the Fe $L_3M_{23}M_{45}$ (~841 eV) peak.

3.3. Inorganic vs organic compounds

The surface of the 90Cu-10Ni alloy is comprised of inorganic species (oxides/hydroxides compounds) and bio-organic compounds, originating from the adlayer (adventitious organic contamination and adsorbed biomolecules of interest). Deciphering changes of the 90Cu-10Ni surface upon immersion in the different media requires a reliable discrimination between organic and inorganic oxygen. This approach has been developed to probing the evolution of passive films and organic compounds adsorbed on stainless steel. [22] The organic portion of oxygen measured by XPS is deduced from the C 1s components due to oxidized carbon (C_{ox}), after the subtraction of the contribution of amines/amides to this C_{ox} signal. By considering that each organic oxygen is in average bound to one carbon, the organic oxygen concentration (O_{org}) may be computed by Eq. (3)

$$O_{org} = C_{ox} - N_{tot} = C_{286.3} + C_{288} + C_{289} - N_{tot} \qquad (3)$$

where the name of an element designates its concentration and the number in subscript designates the binding energy of the peak component. This equation applies strictly if all chemical functions belong to the following series: alcohol (C-OH), primary amine ($C\text{-}NH_2$), ketone and aldehyde (C=O), amide (CO–N–C), ester (CO–O–C). It supposes that ether (C–O–C) or secondary amine (C–N–C) functions are not present in the organic contaminants. If only

carboxylic acid and carboxylate groups, instead of ester, were responsible for the components at about 289 eV and 288 eV, respectively, Eq. 4 should rather be used.

$$O_{org} = C_{ox} - N_{tot} = C_{286.3} + 2\times C_{288} + 2\times C_{289} - N_{tot} \quad (4)$$

It must keep in mind that Eq. (4) is based on considerations of an extreme and not realistic case regarding the nature of the organic adlayer (contaminants, proteins (enzymes), polysaccharides, etc). Considering this equation however allows the parameters deduced from O_{org} to be evaluated critically regarding their dependence to the underlying hypotheses.

Another hypothesis to be considered is that the component at 289 eV may be due to carbonate. [25] The latter may originate from hydrogenocarbonate present in SFW. Table 3 showed that C_{289} was in the range of 1 to 3%, while the Na concentration was below the detection limit for all samples. However, carbonate may be present in the form of Cu hydroxycarbonate [$Cu_2(OH)_2CO_3$]. If C_{289} corresponds to the concentration of the carbon in the form of carbonate, the following equation should be applicable:

$$O_{org} = C_{ox} - N_{tot} = C_{286.1} + C_{288} - N_{tot} \quad (5)$$

Table 3 presents the mole fraction of O_{org} computed according to Eqs. (3), (4), and (5). The mole fraction of inorganic oxygen (O_{inorg}) can thus be deduced by:

$$O_{inorg} = O_{tot} - O_{org} \quad (6)$$

Table 3 shows that the total carbon concentration increased significantly for samples incubated in GAc and GOx media compared to those in SFW and H_2O_2. As shown in Figure 2, in the former media, the C 1s peak shape changed appreciably, indicating a relative increase of the contribution due to carbon bound to oxygen or nitrogen. This is consistent with the evolution of O_{org} which increased independently of the equation used (Table 3).

Figure 4 shows the evolution of the amount of organic compounds with respect to the total inorganic material as a result of the immersion in the different media. These quantities were computed, respectively, as follows:

$$\Sigma_{org} = C + O_{org} + N \quad (7)$$

$$\Sigma_{inorg} = Cu + Ni + O_{inorg} + Cl \quad (8)$$

The incubation of Cu-Ni samples in H_2O_2 medium did not induce noticeable changes on these quantities compared to SFW (typically < 10% difference, Fig. 4A). By contrast, in GAc and GOx media, Σ_{org} strikingly increased and Σ_{inorg} decreased (with a typical difference > 60% and >70%, respectively). These trends were not influenced by the equation used to compute O_{org} (Fig. 4B and C).

3.4. Evolution of the (bio)organic/inorganic interface

The incubation of Cu-Ni samples in different media for 5 days led to significant surface changes which are examined in depth to the regard of both the inorganic adlayer (oxides/hydroxides) and organic adsorbed phase. It is shown that in SFW, the oxide layer is mainly composed of copper oxides/hydroxides, presumably Cu_2O and $Cu(OH)_2$ and Ni hydroxides, namely $Ni(OH)_2$. It must be kept in mind that in some cases, the identification of oxides/hydroxides which form on metallic materials' surfaces may include uncertainties if it is based only on peak decomposition. The photoelectron spectra of transition metals are, indeed, complex owing to (i) the contribution of multiple oxidation states, satellites and spin-orbit coupling and (ii) the uncertainty regarding the baseline. [37] In the present study, the identification of oxides/hydroxides was performed by exploring the position of peaks, the presence/position of satellites and auger parameter (Figures 2 and 3, Table 4). Moreover, a detailed analysis of the literature allowed data to be compared in a reliable way (Table 4). The evolution of the molar concentration of Cu, in its different oxidation states (Cu^{I} and Cu^{II}) and Ni, in the form of Ni^{II}, after incubation in the different media is detailed in Table 3. Results

showed that the immersion in GAc and GOx media causes a significant depletion of Ni and inorganic oxygen, O_{inorg} (increase of O_{org}, see Table 3). By contrast, the concentration of copper (Cu^{I} and Cu^{II}) varied only slightly as a result of immersion in GAc and GOx media.

The weight percentages of elements from the inorganic adlayers are presented in Fig. 5 in the form of a ternary diagram. Each apex of the diagram represents 100 wt. % of Cu, Ni and O_{inorg}. The arrows are perpendicular to the axis indicating the levels of concentration of the corresponding quantity. Results showed that samples incubated in SFW and H_2O_2 are clustered in a narrow domain of composition at a high percentage of O_{inorg}. When samples were incubated in GAc or GOx media, data are also clustered in a narrow domain which is shifted toward lower values of O_{inrog} and Ni, as indicated in Fig. 5 (see arrows 1 and 2, respectively). These findings showed that the composition of the inorganic adlayer formed in H_2O_2 medium is similar to that in SFW, suggesting that the addition of H_2O_2 did not induce any significant oxidation or hydration of the layer in the studied conditions. Also, the composition of the inorganic adlayer was similar in GOx and GAc media and characterized by a higher amount of copper, mostly Cu^{II} (about 68 and 75 % of Cu^{II} in GOx and GAc, respectively), and lower amount of O_{inorg}, compared to SFW and H_2O_2 media. The decrease of Ni and O_{inorg} occurred in a proportion close to a 1:2 relationship, suggesting a depletion of Ni (oxy)hydroxides, consistent with $Ni(OH)_2$ or NiOOH compounds.

In contrast to the inorganic adlayer, i.e. mainly oxides/hydroxides, the nature of the organic adlayer present on the Cu-Ni surface upon natural exposures remains poorly documented. Yet, metal oxides are high-surface-energy solids which tend to reduce the excess interfacial energy through the adsorption of organic compounds (contamination). This process is ubiquitous and may explain why carbon is always detected, at different extent, by XPS analyses on inorganic surfaces. [24] Organic contaminants may originate from different sources, including from material processing or may be adsorbed from the atmosphere during

the cleaning procedure or even from the spectrometer chamber walls. In the present study, the evaluation of organic compounds to the regard of inorganic compounds showed a noticeable increase when samples were immersed in GOx or GAc media (Fig. 4). The evolution of the molar concentration of the contribution of carbon bound to oxygen or nitrogen, $C_{286.3}$, the contribution of oxygen singly bond to carbon, $O_{533.1}$, and nitrogen, N, in the different media is given in Fig. 6. Data were presented in the form of ratios to the sum of organic elements (Σ_{org} = C + O_{org} +N). Results showed that the immersion in GAc and GOx media lead to a noticeable increase of $C_{286.3}/\Sigma_{org}$. This is accompanied by a significant increase of $O_{533.1}/\Sigma_{org}$ in the Gox medium and to a lesser extent in the GAc medium. By contrast, the molar concentration ratios N/Σ_{org} were appreciably low in all the media and remained almost unchanged. These trends suggest that a striking change occurs in the chemical nature of the adsorbed organic compounds when samples are immersed in GOx or GAc media. Moreover, taken together, the evolution of $C_{286.3}/\Sigma_{org}$ and N/Σ_{org} suggest that glucose oxidase did not adsorb on the Cu-Ni surface in a significant amount. The evolution of the molar concentration of nitrogen was indeed not meaningful and could not be correlated with the variations of C 1s components.

Fig. 7A and B address the distribution of carbon among different functional groups, presenting the plots of respectively $C_{286.3}$ and $C_{284.8}$ vs C_{tot}. A clear trend was observed for $C_{286.3}$ showing a significant increase as a result of immersion in GOx or GAc media (Fig. 7A). This is indicative of a surface enrichment with compounds with high oxidized carbon content. By contrast, data due to carbon only bound to carbon and hydrogen, $C_{284.8}$, were scattered around a 1:2 relationship for all samples (Fig. 7B). These observations are at the opposite of those reported for stainless steel surfaces after immersion in solutions of biological interest. Indeed, it was shown that $C_{284.8}$ was the dominating form and its concentration increased linearly with total carbon concentration. [24]

To get more insights into the nature of organic adsorbed compounds, a plot of $C_{286.3}$ vs O_{org} is presented in Fig. 7C for all samples. Linear relationships were obtained independently on the equation used to compute O_{org}, i.e. Eq. 3, 4 or 5 (not shown). This indicates that the component attributed to carbon making a single bond with oxygen or nitrogen, $C_{286.3}$, represents a rather constant proportion of organic oxygen, close to 0.45 for SFW and H_2O_2, and which slightly increased, around 0.54 and 0.75 for GOx and GAc media (Eq. 1, Table 5). This trend was not influenced by the equation used to compute O_{org}, although the variations are sometimes meaningful. Importantly, the $C_{286.3}/O_{org}$ ratio obtained in GOx or GAc media is close to the value of 0.71 expected for pure gluconic acid. This is consistent with an adsorption of gluconic acid, presumably in the form of gluconates (pKa ~ 3.8), on the Cu-Ni surface. Before adding glucose oxidase and glucose, the solution is essentially a H_2CO_3/HCO_3^- buffer with a total 3.15 mM hydrogenocarbonate concentration and a $[HCO_3^-]/[H_2CO_3]$ ratio of about 48. As a result of the addition of the enzyme and glucose, the formation of 1 or 2 mmol/L of H_2O_2, and thus 1 or 2 mmol/L of gluconic acid, is expected to shift the pH from 8 to 6.7 or 6.15, respectively, which is in agreement with the observations (Table 2). The increase of the amount of organic compounds, consistent with gluconic acid, is concomitant with the depletion of the inorganic adlayer in Ni and O_{inorg}. This is consistent with the formation of a hybrid organic-inorganic layer made of copper-gluconate complexes. However, it is not known whether the decrease of the molar concentration of Ni and O_{inorg} results in a screening effect of the hybrid layer (presumably on top of the inorganic layer), or due to a partial removal of copper hydroxides. Gluconic acid forms strong complexes with many transition metals. Evidences of the existence of various Cu^{II}-gluconate complexes have been reported, showing the possible formation of stable chelates with different Cu : gluconate ratios [38, 39]. In the present study, the presence of gluconate may lead to the formation of cupric complexes according to the following reaction:

$$Cu^{2+} + L^{-} = [CuL]^{+} \quad \text{(Eq. 9)}$$

the equilibrium constant of which is equal to logK = 3.06 [40]. The formation of this complex may be explained by the interaction of the Cu^{II} with the carboxylate and α-hydroxyl groups. Furthermore, in basic conditions, the formation of Cu^{II}-gluconate chelates are more favorable to the formation of $Cu(OH)_2$ hydroxide [40]. The formers are indeed stable enough to avoid the formation of the hydroxide.

Complementary information regarding the composition of the adlayer formed in GAc and GOx media is given by means of PM-IRRAS analysis. Results showed, indeed, typical vibrational features of gluconate on the surface of Cu-Ni after incubation in GAc and GOx media, while no bands were observed after incubation in SFW. In the low frequency region, the bands at about 1405 and 1631 cm^{-1} are attributed to the symmetric and antisymmetric stretching modes of the COO^- moiety, respectively. The position of $\nu(COO^-)$ bands are consistent with that observed for copper-gluconate complexes [41]. Also, the band around 1090 cm^{-1} may be attributed to C-O stretching vibration [41, 42]. In the higher frequency region, bands due C-H stretching are visible, and the large band observed around 3500 cm^{-1} is attributed to the stretching vibrations ν(OH) of hydroxyl groups in gluconate. It is worth noting, that this band was only observed on the sample incubated in GAc. The latter sample exhibited, indeed, bands with an overall higher intensity compared to the GOx-incubated sample, probably due to the properties of the oxide layer present on the Cu-Ni that may influence the PM-IRRAS signal.

These findings support the dominating involvement of gluconic acid in surface changes of Cu-Ni upon immersion in GOx medium. By contrast, H_2O_2 seems to have a minor effect although it has a more oxidizing power than oxygen. Accordingly, the biogenic formation of organic acids in natural biofilms clearly deserves particular attention to provide a proper

evaluation of the sustainability of Cu-Ni alloys. This is particularly important in conditions where microbiologically-influenced corrosion and related phenomena are favorable.

4. Conclusion

In this article, an enzymatic model reaction (Eq. 1) was used to mimic an aerobic microbial activity of natural biofilms with the aim to investigate its impact on the surface of a Cu-Ni (90-10) alloy. Samples were incubated for 5 days in aqueous solutions containing the enzyme that generate an oxidizing agent, hydrogen peroxide, and an organic acid, gluconic acid. A detailed analysis of XPS data showed that significant changes of different nature, related to both the inorganic and the organic matter, occur on the surface of Cu-Ni s after immersion. The main change regarding the inorganic phase consists in a significant depletion of the layer with Ni and O_{inorg}. However, the nature of oxides/hydroxides seems to be unchanged. The organic phase was subjected to a striking increase of the amount of organic compounds in the presence of the enzyme, particularly compounds with high oxidized carbon content. Results are consistent with an extensive adsorption of gluconic acid and the formation of a hybrid layer made with copper-gluconate complexes.

The findings described in this paper clearly demonstrate the relevancy of mimicking the biogenic formation of oxidizing and complexing agents, through an enzymatic pathway, for the evaluation Cu-Ni alloy behavior. In future work, it would be most interesting to extend this biomimetic model to other enzymes involved in microbiologically-influenced corrosion. This may be achieved by the identification of (i) extracellular enzymes present in natural biofilms, and (ii) sequential enzymatic reactions or other enzyme-mediated pathways that may impact the sustainability of the Cu-Ni materials.

References

[1] F. Mansfeld, The interaction of bacteria and metal surfaces, Electrochimica Acta, 52 (2007) 7670-7680.
[2] B.J. Little, J.S. Lee, R.I. Ray, The influence of marine biofilms on corrosion: A concise review, Electrochimica Acta, 54 (2008) 2-7.
[3] I.B. Beech, J. Sunner, Biocorrosion: towards understanding interactions between biofilms and metals, Current Opinion in Biotechnology, 15 (2004) 181-186.
[4] I.B. Beech, Corrosion of technical materials in the presence of biofilms—current understanding and state-of-the art methods of study, International Biodeterioration & Biodegradation, 53 (2004) 177-183.
[5] J. Landoulsi, C. Dagbert, C. Richard, R. Sabot, M. Jeannin, K. El Kirat, S. Pulvin, Enzyme-induced ennoblement of AISI 316L stainless steel: Focus on pitting corrosion behavior, Electrochimica Acta, 54 (2009) 7401-7406.
[6] F. Mansfeld, G. Liu, H. Xiao, C.H. Tsai, B.J. Little, The corrosion behavior of copper alloys, stainless steels and titanium in seawater, Corrosion Science, 36 (1994) 2063-2095.
[7] F. Mansfeld, B. Little, Microbiologically influenced corrosion of copper-based materials exposed to natural seawater, Electrochimica Acta, 37 (1992) 2291-2297.
[8] J. Landoulsi, K.E. Kirat, C. Richard, D. Féron, S. Pulvin, Enzymatic Approach in Microbial-Influenced Corrosion: A Review Based on Stainless Steels in Natural Waters, Environmental Science & Technology, 42 (2008) 2233-2242.
[9] J. Landoulsi, K.E. Cooksey, V. Dupres, Review – Interactions between diatoms and stainless steel: focus on biofouling and biocorrosion, Biofouling, 27 (2011) 1105-1124.
[10] S.J. Yuan, A.M.F. Choong, S.O. Pehkonen, The influence of the marine aerobic Pseudomonas strain on the corrosion of 70/30 Cu–Ni alloy, Corrosion Science, 49 (2007) 4352-4385.
[11] N.O. San, H. Nazır, G. Dönmez, Microbial corrosion of Ni–Cu alloys by Aeromonas eucrenophila bacterium, Corrosion Science, 53 (2011) 2216-2221.
[12] N.O. San, H. Nazır, G. Dönmez, Microbially influenced corrosion and inhibition of nickel–zinc and nickel–copper coatings by Pseudomonas aeruginosa, Corrosion Science, 79 (2014) 177-183.
[13] W.H. Dickinson, Z. Lewandowski, R.D. Geer, Evidence for Surface Changes During Ennoblement of Type 316L Stainless Steel: Dissolved Oxidant and Capacitance Measurements, CORROSION, 52 (1996) 910-920.
[14] K. Xu, S.C. Dexter, G.W.L. III, Voltammetric Microelectrodes for Biocorrosion Studies, CORROSION, 54 (1998) 814-823.

[15] N. Washizu, Y. Katada, T. Kodama, Role of H2O2 in microbially influenced ennoblement of open circuit potentials for type 316L stainless steel in seawater, Corrosion Science, 46 (2004) 1291-1300.
[16] W. Wang, X. Zhang, J. Wang, The influence of local glucose oxidase activity on the potential/current distribution on stainless steel: A study by the wire beam electrode method, Electrochimica Acta, 54 (2009) 5598-5604.
[17] N.B. Bhosle, P.D. Sankaran, A.B. Wagh, Carbohydrate sources of microfouling material developed on aluminium and stainless steel panels, Biofouling, 2 (1990) 151-164.
[18] J. Landoulsi, M.J. Genet, C. Richard, K. El Kirat, P.G. Rouxhet, S. Pulvin, Ennoblement of stainless steel in the presence of glucose oxidase: Nature and role of interfacial processes, Journal of Colloid and Interface Science, 320 (2008) 508-519.
[19] J.T. Yates, Infrared Spectroscopy, in: J.T. Yates Jr (Ed.) Experimental Innovations in Surface Science: A Guide to Practical Laboratory Methods and Instruments, Springer International Publishing, Cham, 2015, pp. 321-332.
[20] C. Bourdillon, V. Thomas, D. Thomas, Electrochemical study of d-glucose oxidase autoinactivation, Enzyme and Microbial Technology, 4 (1982) 175-180.
[21] M. Yoshimoto, Y. Miyazaki, M. Sato, K. Fukunaga, R. Kuboi, K. Nakao, Mechanism for High Stability of Liposomal Glucose Oxidase to Inhibitor Hydrogen Peroxide Produced in Prolonged Glucose Oxidation, Bioconjugate Chemistry, 15 (2004) 1055-1061.
[22] J. Landoulsi, M.J. Genet, C. Richard, K. El Kirat, S. Pulvin, P.G. Rouxhet, Evolution of the passive film and organic constituents at the surface of stainless steel immersed in fresh water, Journal of Colloid and Interface Science, 318 (2008) 278-289.
[23] P.G. Rouxhet, M.J. Genet, XPS analysis of bio-organic systems, Surface and Interface Analysis, 43 (2011) 1453-1470.
[24] J. Landoulsi, M.J. Genet, S. Fleith, Y. Touré, I. Liascukiene, C. Méthivier, P.G. Rouxhet, Organic adlayer on inorganic materials: XPS analysis selectivity to cope with adventitious contamination, Applied Surface Science, 383 (2016) 71-83.
[25] NIST X-ray Photoelectron Spectroscopy Database NIST Standard Reference Database 20, Version 4.1 (Web Version), http://srdata.nist.gov/xps/, in.
[26] S. Poulston, P.M. Parlett, P. Stone, M. Bowker, Surface Oxidation and Reduction of CuO and Cu2O Studied Using XPS and XAES, Surface and Interface Analysis, 24 (1996) 811-820.
[27] C. Wagner, W. M. Riggs, L. E. Davies, J. F. Moulder, G.E. Muilenburg, in: Handbook of X-ray Photoelectron Spectroscopy, Perkin-Elmer, Eden Prairie, MN, 1979, pp. 74-80.
[28] S.W. Goh, A.N. Buckley, R.N. Lamb, R.A. Rosenberg, D. Moran, The oxidation states of copper and iron in mineral sulfides, and the oxides formed on

initial exposure of chalcopyrite and bornite to air, Geochimica et Cosmochimica Acta, 70 (2006) 2210-2228.
[29] W.M. Skinner, C.A. Prestidge, R.S.C. Smart, Irradiation Effects During XPS Studies of Cu(II) Activation of Zinc Sulphide, Surface and Interface Analysis, 24 (1996) 620-626.
[30] S.K. Chawla, N. Sankarraman, J.H. Payer, Diagnostic spectra for XPS analysis of copper-oxygen-sulfur-hydrogen system compounds, J. Electron Spectrosc. Relat. Phenom., 61 (1992) 1-18.
[31] N.S. McIntyre, M.G. Cook, X-ray photoelectron studies on some oxides and hydroxides of cobalt, nickel, and copper, Anal. Chem., 47 (1975) 2208-2213.
[32] M.C. Biesinger, L.W.M. Lau, A.R. Gerson, R.S.C. Smart, Resolving surface chemical states in XPS analysis of first row transition metals, oxides and hydroxides: Sc, Ti, V, Cu and Zn, Applied Surface Science, 257 (2010) 887-898.
[33] C.D. Wagner, Auger lines in x-ray photoelectron spectrometry, Analytical Chemistry, 44 (1972) 967-973.
[34] G. Moretti, Auger parameter and Wagner plot in the characterization of chemical states by X-ray photoelectron spectroscopy: a review, Journal of Electron Spectroscopy and Related Phenomena, 95 (1998) 95-144.
[35] Y.Z. Wang, A.M. Beccaria, G. Poggi, The effect of temperature on the corrosion behaviour of a 70/30 Cu-Ni commercial alloy in seawater, Corrosion Science, 36 (1994) 1277-1288.
[36] W.F.S. J.F. Moulder, P.E. Sobol, K.D. Bomben, Handbook of X-ray Photoelectron Spectroscopy, Perkin-Elmer Corp, Eden Prairie, MN, , 1992.
[37] C. Fadley, Basic concepts of X-ray photoelectron spectroscopy, Electron spectroscopy: theory, techniques and applications, 2 (1978) 1-156.
[38] D.T. Sawyer, Metal-Gluconate Complexes, Chemical Reviews, 64 (1964) 633-643.
[39] R.L. Pecsok, R.S. Juvet, The Gluconate Complexes. I. Copper Gluconate Complexes in Strongly Basic Media1, Journal of the American Chemical Society, 77 (1955) 202-206.
[40] G.M. Escandar, L.F. Sala, Complexes of Cu(II) with D-aldonic and D-alduronic acids in aqueous solution, Canadian Journal of Chemistry, 70 (1992) 2053-2057.
[41] G.M. Escandar, J.M. Salas Peregrin, M. Gonzalez Sierra, D.b. Martino, M. Santoro, A.A. Frutos, S.I. Garci´a, G. Labadie´, L.F. Sala, Interaction of divalent metal ions withd-gluconic acid in the solid phase and aqueous solution, Polyhedron, 15 (1996) 2251-2261.
[42] B. Beden, F. Largeaud, K.B. Kokoh, C. Lamy, Fourier transform infrared reflectance spectroscopic investigation of the electrocatalytic oxidation of d-glucose: Identification of reactive intermediates and reaction products, Electrochimica Acta, 41 (1996) 701-709.

Table 1. Chemical bulk composition of 90Cu-10Ni alloy (wt.%).

	C	Fe	Mn	Ni	P	Pb	S	Sn	Zn	Cu
wt.%	0.004	1.65	0.78	10.31	0.002	0.003	0.003	0.009	0.014	balance

Table 2. Characteristics of the solutions used in this study.

	Hydrogen peroxide (mM)	Gluconic acid (mM)	pH *
SFW	-	-	8.1
H_2O_2	2	-	8.2
GAc	-	2	6.4
Gox	~ 2 †	~ 2 ‡	7.2

* Measured after 5 days of immersion
† Measured after 5 days of immersion (data from Figure 1B)
‡ Expected value (Eq. 1)

Table 3. Surface Concentrations (Mole Percentages Computed over All Elements except Hydrogen) of Elements Determined by XPS.

	$C_{284.8}$	$C_{286.3}$	C_{288}	C_{289}	$\mathbf{C_{tot}}$	$\mathbf{N_{tot}}$	$O_{529.7}$	$O_{531.2}$	$O_{533.1}$	$\mathbf{O_{tot}}$	O_{org}			Cu^{I}	Cu^{II}	$\mathbf{Cu_{tot}}$	$\mathbf{Ni_{tot}}$	**Cl**
											Eq.3	Eq.4	Eq.5					
SFW	32.41	5.15	3.67	1.95	**43.17**	**0.51**	3.11	31.41	3.94	**38.47**	10.25	15.87	8.30	3.99	6.35	**10.34**	**6.90**	**0.56**
H_2O_2	34.27	5.05	4.58	2.32	**46.21**	**0.40**	2.34	31.32	3.38	**37.05**	11.54	18.43	9.22	3.07	6.75	**9.82**	**5.90**	**0.56**
GAc	31.35	20.34	6.29	1.02	**59.01**	**0.38**	0.72	22.38	6.36	**29.46**	27.28	34.60	26.26	2.46	7.58	**10.04**	**0.88**	**0.24**
Gox	26.01	20.25	7.70	2.75	**56.71**	**0.67**	0.11	18.77	12.97	**31.84**	30.03	40.48	27.28	3.52	7.04	**10.56**	**0.14**	**0.09**

Table 4. Binding energies (BE) and kinetic energies (KE) measured on Cu $2p_{3/2}$ and Cu $L_3M_{45}M_{45}$ peaks, respectively, and the corresponding Auger parameters α'_{Cu}.

	Cu $2p_{3/2}$ (BE, eV) †	**Cu $2p_{3/2}$ (BE, eV)** ‡	**Cu $L_3M_{45}M_{45}$ (KE, eV)**	**α' (eV)** §	**α' (eV)** #
SFW	932.2 (0.05)	934.28 (0.28)	916.7 (0.12)	1849.04 (0.49)	1851.12 (0.49)
H_2O_2	932.3 (0.09)	934.35 (0.25)	916.6 (0.19)	1848.89 (0.39)	1850.92 (0.39)
GAc	932.4 (0.00)	934.25 (0.00)	916.3 (0.00)	1848.94 (0.00)	1850.79 (0.00)
Gox	932.9 (0.30)	934.57 (0.21)	916.3 (1.05)	1849.34 (0.75)	1850.95 (0.75)
Cu *	932.61 (0.20)	-	918.61 (0.23)	1851.22 (0.16)	-
Cu_2O *	932.45 (0.23)	-	916.70 (0.30)	1849.19 (0.32)	-
CuO *	-	933.71 (0.43)	917.80 (0.28)	-	1851.49 (0.35)
$Cu(OH)_2$ *	-	934.23 (1.06)	916.80 (0.00)	-	1851.30 (0.00)

* Data from [25]
† Component at the lowest binding energy
‡ Component at the highest binding energy
§ Computed using the component at the lowest binding energy
# Computed using the component at the highest binding energy

Table 5. Proportion of oxidized carbon which makes a single bond with oxygen or nitrogen, $C_{286.3}$, ratioed to the organic oxygen concentration, O_{org}, as computed y Eq. 3; 4 or 5, as indicated. Statistical data for different sets of samples.

Incubation medium	**$C_{286.3}$ / O_{org}**		
	Eq. 3	Eq. 4	Eq. 5
SFW	0.48 (0.14)	0.31 (0.12)	0.60 (0.16)
H_2O_2	0.41 (0.16)	0.26 (0.12)	0.51 (0.18)
GOx	0.54 (0.09)	0.40 (0.10)	0.60 (0.09)
GAc	0.75 (0.00)	0.59 (0.00)	0.77 (0.00)

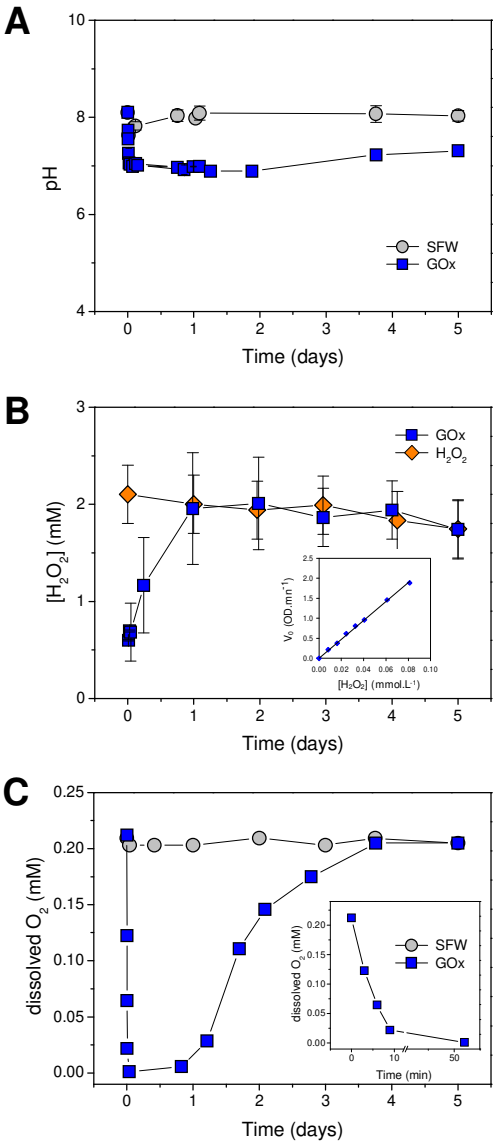

Fig. 1. Evolution of (A) pH, (B) concentration of H_2O_2, [H_2O_2], and (C) dissolved O_2 as function of time during 5 days in (●) SFW, (◆) H_2O_2 and (■) GOx media, as indicated. (B, inset) relationship between the activity of peroxidase (initial velocity V_0) and the concentration of H_2O_2.

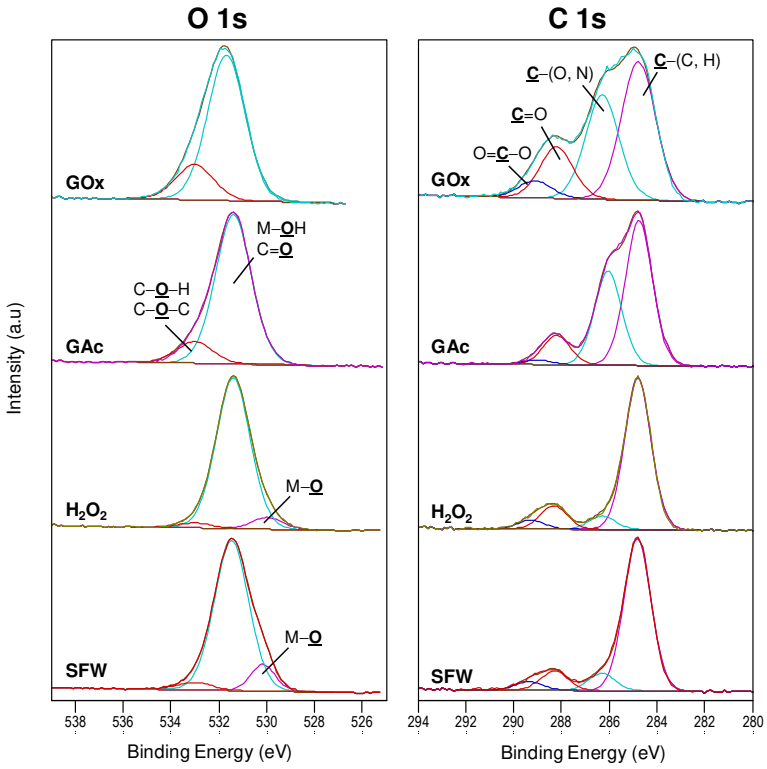

Fig. 2. Representative O1s and C1s peaks recorded on 90Cu-10Ni samples after immersion period of 5 days in the different media: SFW, H_2O_2, GAc and GOx.

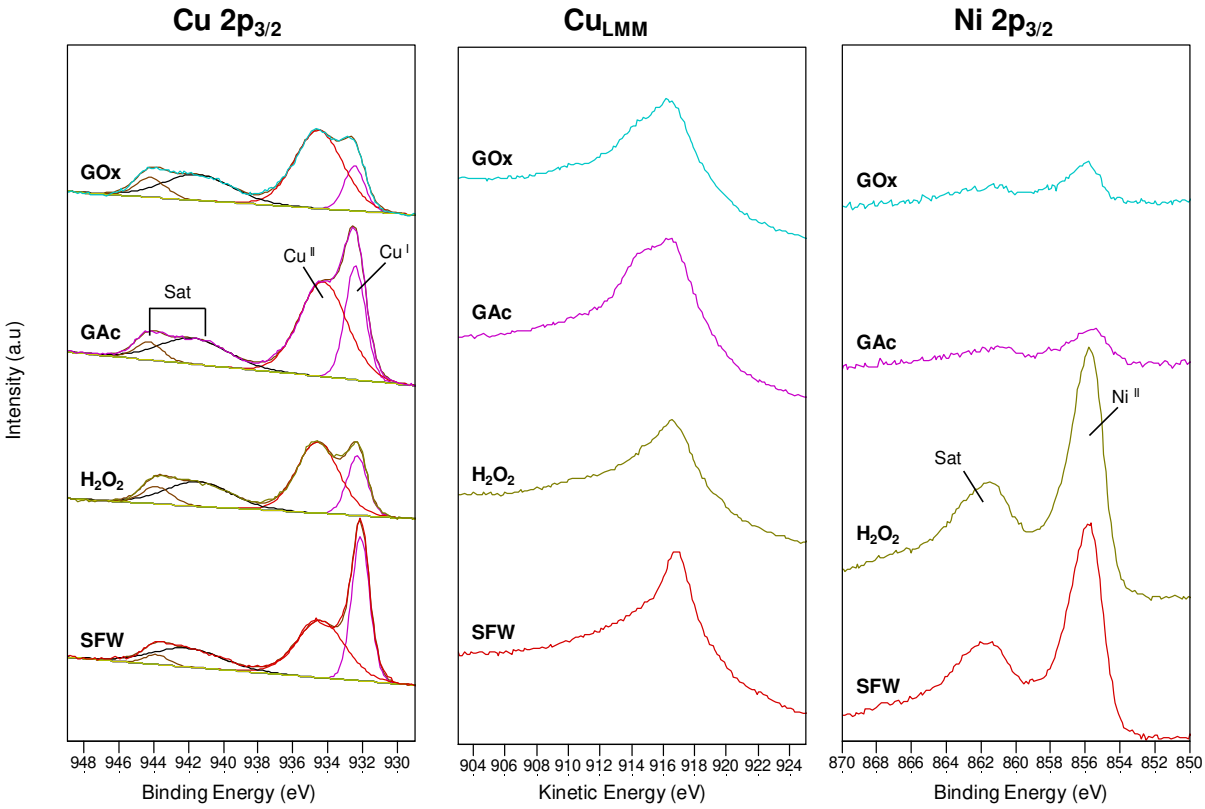

Fig. 3. Representative Cu $2p_{3/2}$, Cu $L_3M_{45}M_{45}$ and Ni $2p_{3/2}$ peaks recorded on 90Cu-10Ni samples after immersion period of 5 days in the different media: SFW, H_2O_2, GAc and GOx.

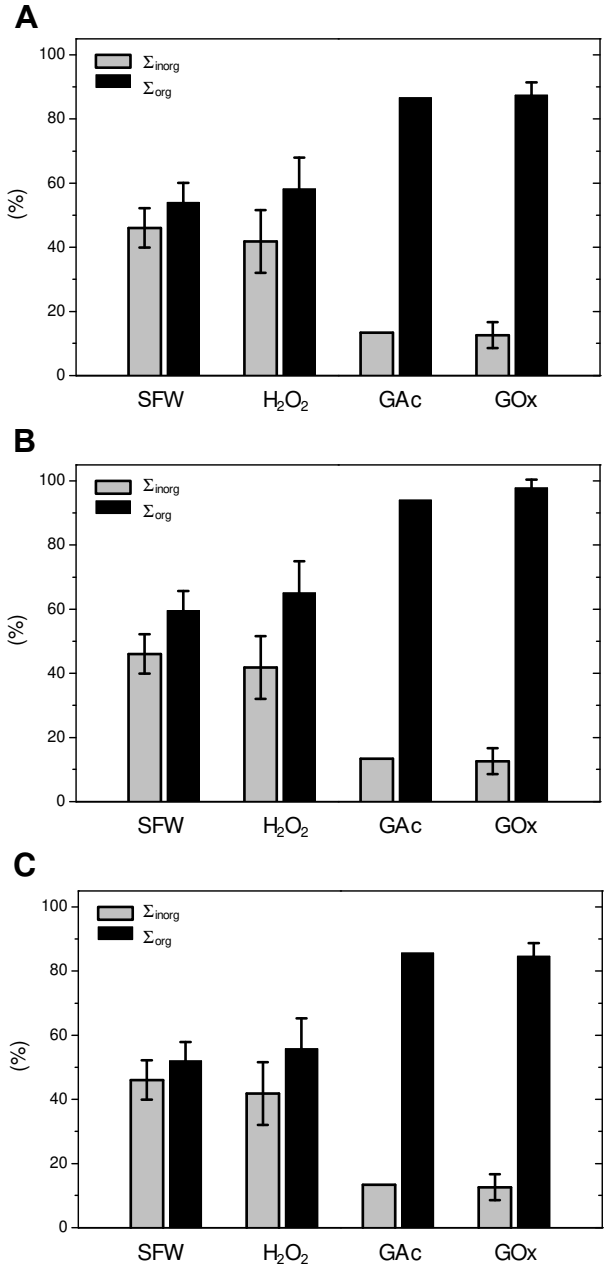

Fig. 4. Evolution of the molar concentration ratio of the sum of organic elements (Σ_{org} = C + O_{org} + N) and the sum of inorganic elements (Σ_{inorg} = Cu + Ni + O_{inorg} + Cl) measured by XPS (data from Table 3), on 90Cu-10Ni samples after immersion period of 5 days in SFW, H_2O_2, GAc and GOx. O_{org} was computed using (A) Eq. (3), (B) Eq. (4) and (C) Eq. (5). The standard variations are the mean value of 3 independent measurements.

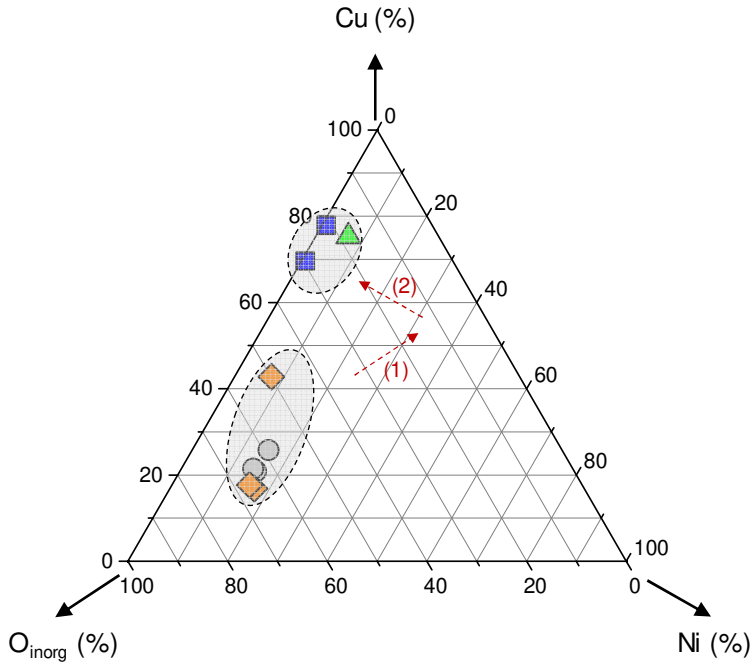

Fig. 5. Ternary diagrams presenting the sums of mole fractions determined by XPS: (A) elements related to the inorganic matter Cu, Ni and other inorganic compounds ($\Sigma_{oth.inorg}$) on 90Cu-10Ni samples after immersion in SFW (●), H_2O_2 (◆), GAc (▲) and GOx (■). O_{inorg} was computed using Eq. 6 and O_{org} using Eq. 3.

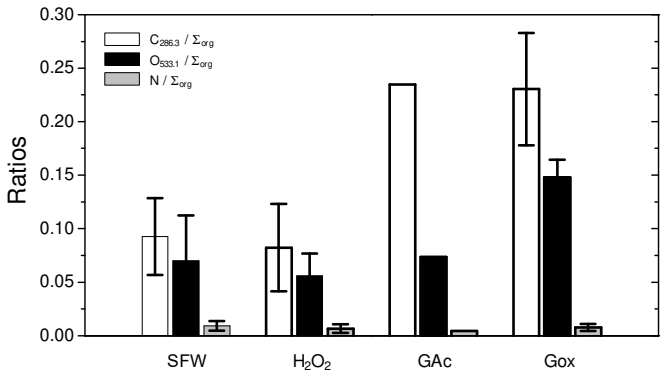

Fig. 6. Evolution of the molar concentrations ratioed to the sum of organic elements (Σ_{org} = C + O_{org} + N) measured by XPS (data from Table 3) on 90Cu-10Ni samples after immersion

period of 5 days in SFW, H_2O_2, GAc and GOx. The standard variations are the mean value of 3 independent measurements.

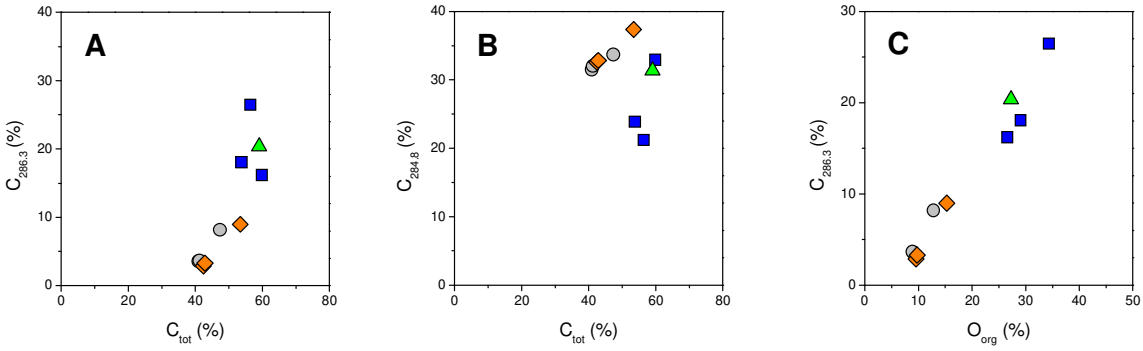

Fig. 7. Relationship between molar concentrations measured by XPS recorded on 90Cu-10Ni samples after immersion in SFW (●), H_2O_2 (◆), GAc (▲) and GOx (■). O_{org} was computed using Eq. 3: (A) $C_{286.3}$ *vs* C_{tot}, (B) $C_{284.8}$ *vs* C_{tot}, (A) $C_{286.3}$ *vs* O_{org}.

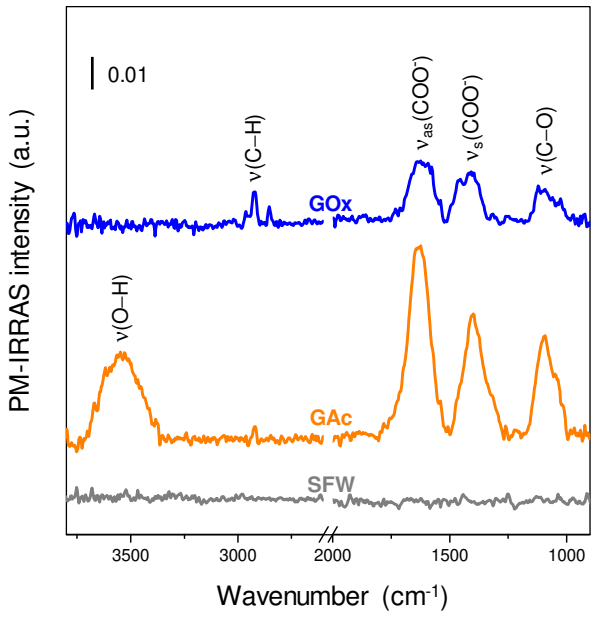

Fig. 8. PM-IRRAS spectra recorded on on 90Cu-10Ni samples after immersion period of 5 days in SFW, GAc and GOx, as indicated.

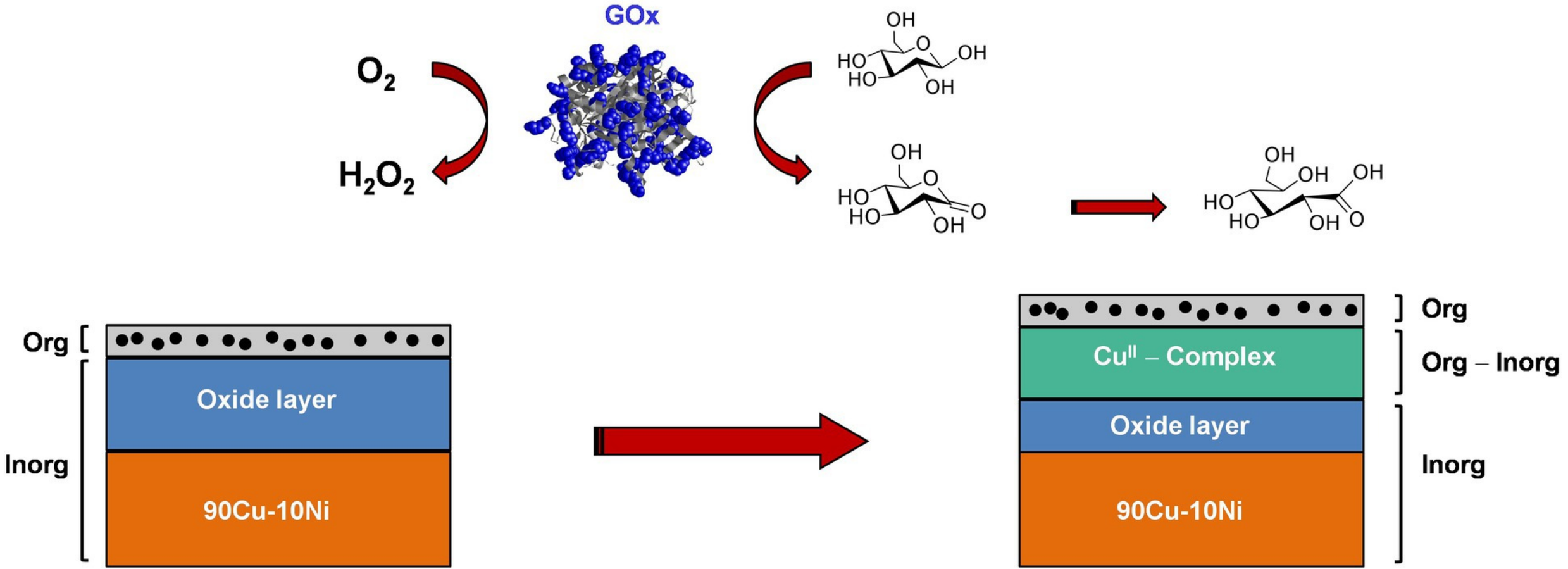
GOx
O2
H2O2
OH
HO
O
Org
Oxide layer
Inorg
90Cu-10Ni
CuII – Complex
Org – Inorg